

Article

# Reductions in the Laser Welding Deformation of STS304 Cylindrical Structure Using the Pre-Stress Method

Se-Hwan Lee <sup>1</sup>, Ho-Chan Jeon <sup>1</sup> and Jeong-Ung Park <sup>2,\*</sup> 

<sup>1</sup> The 1st R & D Institute, Agency for Defense Development, Yuseong-gu, Daejeon 34186, Republic of Korea

<sup>2</sup> Department of Civil Engineering, Chosun University, Gwangju 61452, Republic of Korea

\* Correspondence: jupark@chosun.ac.kr

**Abstract:** Welding deformation occurs due to non-uniform thermal expansion, thermal contraction, restraint, and phase transformation in a metal by a local welding heat source. This causes problems such as low buckling strength and the reduced workability of the production process. Correcting welding deformations in stainless steel using heat—such as by linear heating—causes metal sensitization, which should be avoided. Herein, welding deformation was reduced by applying tension stress instead of correcting the deformation by heating. A deformation-prevention jig was used to reduce welding deformation during the manufacturing of a cylinder made of STS304 by laser welding. The tensile stress was induced by pushing the cylinder shell outward using the deformation-prevention jig. A thermo-elastoplastic analysis was performed to investigate the effects of the magnitude of the tensile stress on welding deformation. Furthermore, the parametric results—which indicated a reduction in welding deformation—were verified through experiments. The thermo-elastoplastic analysis suggested that deformation did not occur when the magnitude of tensile stress was approximately 50% of the yield stress of the base metal. Moreover, the deformation was experimentally reduced by 11–20% when a tensile stress of 30 MPa was applied to the cylinder, compared with that in the absence of tensile stress.

**Keywords:** welding deformation; welding deformation-prevention jig; cylindrical structures; STS304; laser welding; pre-stress method; thermo-elastoplastic analysis



**Citation:** Lee, S.-H.; Jeon, H.-C.; Park, J.-U. Reductions in the Laser Welding Deformation of STS304 Cylindrical Structure Using the Pre-Stress Method. *Metals* **2023**, *13*, 798. <https://doi.org/10.3390/met13040798>

Academic Editors: João Pedro Oliveira, Miguel Cervera and Wei Zhou

Received: 30 January 2023

Revised: 20 March 2023

Accepted: 11 April 2023

Published: 18 April 2023



**Copyright:** © 2023 by the authors. Licensee MDPI, Basel, Switzerland. This article is an open access article distributed under the terms and conditions of the Creative Commons Attribution (CC BY) license (<https://creativecommons.org/licenses/by/4.0/>).

## 1. Introduction

Welding deformations are caused by non-uniform thermal expansion and contraction by local welding heat sources during the manufacturing of welded structures, such as ships, bridges, and aircraft. These contractions and expansions cause plastic deformation owing to internal and external restraints, which appear as welding residual stresses and deformations. Welding deformation is particularly affected by the various shapes of welded structures, welding sequences, and welding conditions [1,2].

Laser welding, which is used to create complex structures and parts with high precision, has recently received increasing attention in the field of additive manufacturing. Ref. [3] printed a Ti–Ni–Ti-like sandwich structure using the direct energy deposition method. A laser beam was used to melt and fuse layers of Ti and Ni to create a sandwich structure with unique properties, such as high strength and shape memory. Ref. [4] developed a model to predict the deformation of a lattice support structure in the laser-powder bed fusion additive manufacturing process using the eigenstrain method and efficiently predicted the deformation and residual stress. Ref. [5] investigated the effects of direct aging and annealing on the microstructure and mechanical properties of Al–Si–10Mg, produced by selective laser melting. A laser was used to melt and fuse layers of an Al–Si alloy to create a part with high strength and excellent corrosion resistance. Ref. [6] developed an anti-deformation model to improve the manufacturing accuracy of built-in channels using selective laser melting and demonstrated that increased channel length and depth led to increased deformation and decreased distortion, respectively.

When the shape of a welded structure is cylindrical (as in this study), and bending occurs on the appearance of the structure owing to welding deformation [7,8], it causes aerodynamic resistance as well as affecting other structures in the manufacturing process because of the mismatch in the welded part. These welding deformations generally occur in thin structures rather than in thick structures [9]. Therefore, laser welding with a low heat input is performed in thin-plate structures to minimize welding deformation. However, welding deformation—depending on the shape and welding position of the welded structure—cannot be avoided. Various studies have been conducted to predict or prevent welding deformation by analyzing the generation mechanism of welding deformation [10,11]. Methods to prevent welding deformation include the inverse deformation method [12], cooling method [13], welding sequence method [14], and pre-stress method [15,16]. The effects of the anti-deformation methods depend on the shape, thickness, and welding process of the structure. Therefore, these methods should be selected carefully based on the characteristics of the welded structure.

Ref. [17] used a numerical analysis method to minimize welding deformation during circumferential welding by splitting the entire weld length and measuring the change in diameter at three locations in the weld. When the total welding length was further divided, the diametrical welding deformation decreased. Ref. [15] confirmed sensitization at the welded part when linear heating was used to correct welding deformation during the manufacturing of a vacuum container with STS304. Therefore, the tensile method was analytically investigated to minimize welding deformation instead of correcting this via linear heating. The transverse shrinkage and angular strain were reduced by 80% when the tensile stress was approximately 0.05% of the yield stress of the parent metal.

Ref. [18] analyzed welding deformation and identified the causes of its occurrence to control the deformation during the manufacturing of a cylindrical welded structure with a diameter of approximately 22 mm, which was used for an offshore plant platform. The entire welding length in the circumferential direction was divided into small sections, and thermo-elastoplastic analysis was performed to analyze and control the deformation behavior. Consequently, the magnitude of deformation was significantly reduced in the case of back-step welding; however, no significant difference was observed in deformation reduction by split welding when the total length of the welded part was divided into four or eight sections. The lowest welding deformation occurred when the total welding length was divided into four sections and symmetrically welded simultaneously.

Ref. [19] derived a relationship between welding deformation and restraint in fillet and butt welds. The degree of restraint was determined through experiments and finite-element analysis. A welding deformation prediction system was developed based on the deformation sequence of large steel structures. In other studies, the effects of welding deformation-prevention jigs were investigated for minimizing welding deformation in construction machinery structures by changing the position and spacing of the constraint jigs. [20–24] performed finite-element analysis to investigate the effect of clamp removal time on the welding residual stress and welding deformation during the one-pass butt welding of an STS304-based structure. The residual stress and angular deformation were slightly affected by the removal of the clamp immediately after welding was completed. However, when the clamp was removed once the temperature of the welded part reached room temperature, the residual stress was opposite to that in the free state and welding deformation barely occurred.

Studies on planar structures and arc welding processes have been widely reported in the literature [22,25]; however, studies on preventing deformation during laser welding of cylindrical structures by thermo-elastoplastic analysis are not available—except for the one reported by Lee et al., 2020. Furthermore, studies on preventing deformation during the laser welding of thin cylindrical structures [26] are limited. In addition, the reduction effect of welding deformation using thermo-elastoplastic analysis was examined through simulation by Ref. [27]; therefore, experimental investigations on its field applicability are required.

Herein, a deformation-prevention jig that pushes the cylindrical shell from the inside of the cylinder was developed and reductions in welding deformation during the manufacturing of a cylindrical structure with STS304 by laser welding was confirmed through experiments. Furthermore, experiments were conducted with and without pre-stress to investigate the effects of tensile stress on welding deformation. The results were compared with the results of a thermo-elastoplastic analysis reported in literature. The results obtained through experimental and thermo-elastoplastic analysis indicated that tensile stress can be induced in the actual cylinder and welding deformation can be reduced using a welding deformation-prevention jig.

## 2. Transient Thermo-Elastoplastic Analysis Using the Pre-Stress Method

A thermo-elastoplastic analysis was conducted using the 1/4 analysis model (Figure 1a) to reduce deformation occurring at the seam weld of the cylindrical steel structure [27]. The length and radius (R) of the analysis model were 600 and 570 mm, respectively. The thicknesses of the skin and back plates were 2.5 and 2 mm, respectively. The skin and back plates were fastened using fasteners at intervals of 100 mm.

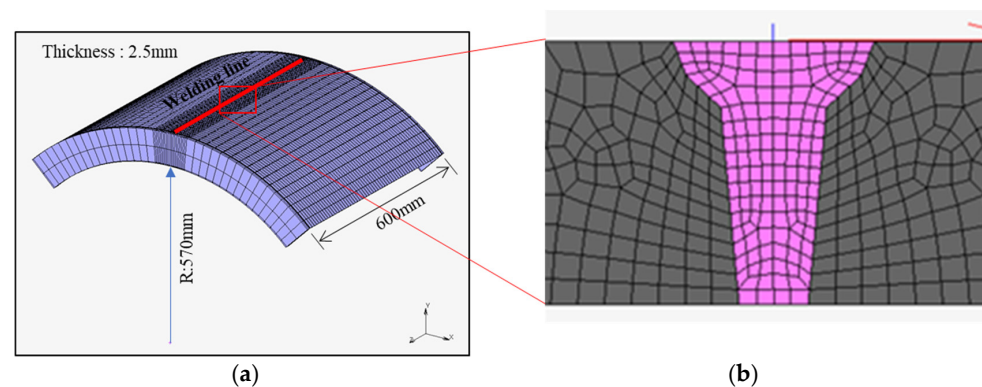


**Figure 1.** Analysis model: (a) Shape and dimension of model; (b) mesh shape [27].

To reduce the welding deformation, a forced displacement was applied from the inside to the outside to expand the cylindrical shell, and tensile stresses of 0, 50, 100, and 140 MPa were achieved on the skin plate. Figure 1b shows the mesh shape of the weld, which was used to model the weld in the thermo-elastoplastic analysis.

STS 304 steel was used in the analysis. Laser welding was performed at 2500 W with a welding speed of 2000 mm/min. The yield strength of the steel was 265 MPa at room temperature, tensile strength was 650 MPa, elongation was 60%, and the coefficient of linear expansion was  $1.6 \times 10^{-5}$  ( $1/^\circ\text{C}$ ). The temperature-dependent physical and mechanical properties of STS304 steel are shown in Figure 2 [27].

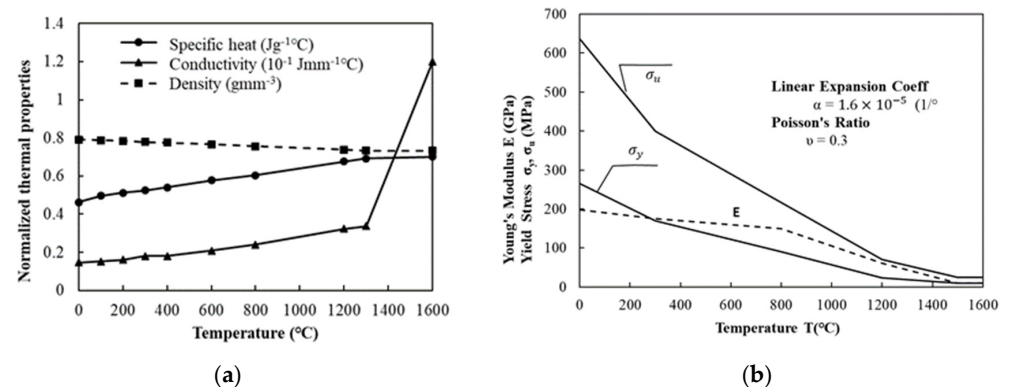


**Figure 2.** Temperature-dependent material properties of STS304: (a) physical properties; (b) mechanical properties.

To model the welding heat source, the weld flux, weld filler, and weld path options were selected in the MSC Marc 2017 software [28]. A three-dimensional eight-node full-integration element model was used. The welding heat source [29] was modeled as a volumetric heat source (Figure 3) using the heat source Equation (1). Data on the welding width and depth were selected based on the cross-section of the welded specimen. The welding line was set with the weld path option, and a welding wire was created when the welding heat source was moved using the weld filler option.

$$q_f(x, y, z, t) = \frac{6\sqrt{3}f_f Q}{abc_f \pi \sqrt{\pi}} \exp\left(-3\left(\frac{x^2}{a^2} + \frac{y^2}{b^2} + \frac{(z - \gamma t)^2}{c_f^2}\right)\right) \quad (1)$$

$$q_r(x, y, z, t) = \frac{6\sqrt{3}f_r Q}{abc_r \pi \sqrt{\pi}} \exp\left(-3\left(\frac{x^2}{a^2} + \frac{y^2}{b^2} + \frac{(z - \gamma t)^2}{c_r^2}\right)\right) \quad (2)$$

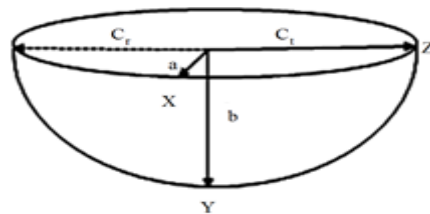


**Figure 3.** Volumetric weld flux [27].

where

$q_f$ : volumetric heat input per unit of the front molten pool

$q_r$ : volumetric heat input per unit of the rear molten pool.

$Q = \eta VI$ : total heat input

$a$ :  $x$  direction welding width

$b$ :  $y$  direction welding depth

$c_f$ : forward molten pool length in  $z$  direction

$c_r$ : rear molten pool length in  $z$  direction

$f_f, f_r$ : dimensionless numbers

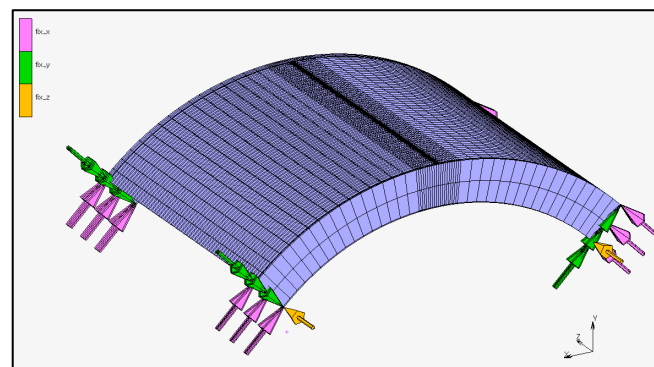
$\eta$ : efficiency

$V$ : voltage

$I$ : current

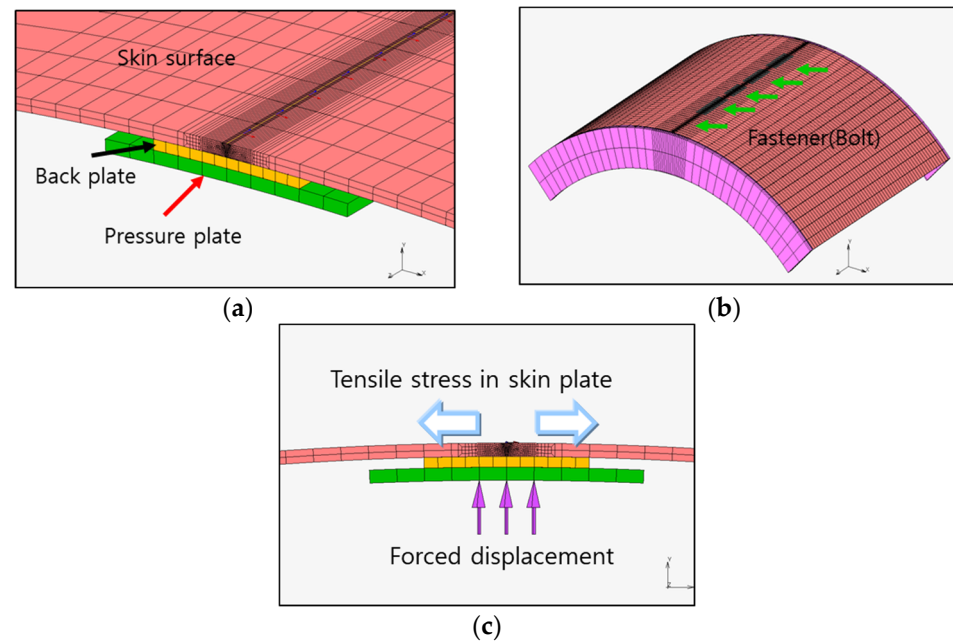
$$f_f = \frac{2}{1 + c_r/c_f}, \quad f_r = \frac{2}{1 + c_f/c_r} \quad (3)$$

Figure 4 shows the boundary conditions used in the analysis; only the upper and lower frame sections were constrained under symmetric conditions using the local coordinates, whereas the skin plate was not constrained [27].



**Figure 4.** Boundary condition for seam welding [27].

The deformation that occurred during the seam welding of the cylinder was caused by welding from the inside of the cylinder. This type of deformation is the sum of the angular deformation caused by the temperature difference between the surface and the lower section of the welded part and the longitudinal bending deformation based on the position of the neutral axis of the member. An inverse deformation or a pre-stress method was used to effectively prevent such welding deformations. Therefore, the shell was extruded from the inside to the outside during the thermo-elastoplastic analysis to induce a tensile stress on the shell. The tensile stress was applied to the shell in the thermo-elastoplastic analysis to reduce deformation (Figure 5).



**Figure 5.** Modeling of pre-stress method: (a) pressure plate; (b) bolting; (c) forced displacement [27].

Figure 5a demonstrates the skin, back, and pressure plates. Tensile stress was induced on the skin plate by applying displacement from the inside of the cylinder. The skin plate has a seam weld, whereas the pressure plate is a rigid element that facilitates a forced displacement and is in contact with the back plate. As shown in Figure 5b, the skin and back plates are connected to fasteners (bolts) at intervals of 100 mm in the direction of the welding line. In the thermo-elastoplastic analysis, the fastener was modeled as attached using the *glue* option available in the MSC Marc 2017 software. In addition, a pressure plate was modeled to impose a forced displacement (Figure 5c). The pressure plate transmits a forced displacement to the skin plate through contact with the back plate. The forced displacement is gradually applied before welding and subsequently removed when the welding is completed, and the welded part reaches room temperature (25 °C).

### 3. Experimental Work

#### 3.1. Specimen Preparation

Two specimens were manufactured to experimentally investigate the effect of pre-stressing methods on the reduction of welding deformations. Figure 6 demonstrates the shape and dimensions of the specimens; the only difference between the two specimens was the thickness of the skin plate, which was 2.0 and 2.67 mm. The diameter and length of the specimens were 377 and 240 mm, respectively. One seam weld and three stiffener welds were used. The frames were installed on both ends of the circularly rolled skin plate. Moreover, a flat plate stiffener was placed inside the seam and stiffener welds, and the skin plate and plate stiffener were fastened using three fasteners at 100 mm intervals. Similar to bead-on-plate welding, a heat source passed through the skin plate in the stiffener welding

process and was welded to the flat plate stiffener installed inside. The length of each stiffener weld was 60 mm.

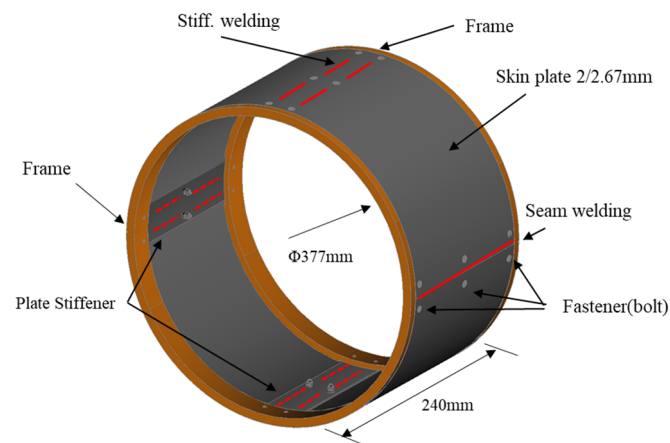


**Figure 6.** Specimen used in experiment and analysis.

Table 1 lists the chemical composition of the STS304 material used in the experiments and the thermo-elastoplastic analysis. Table 2 lists the laser welding conditions, with nitrogen as a protective gas at a flow rate of 25 L/min. Figure 7 depicts the laser welding state. Figure 8 shows a cross-sectional macrograph of stiffener welding joints. Figure 8a shows a skin thickness of 2.0 mm and a stiffness thickness of 2.0 mm, and Figure 8b shows a skin thickness of 2.67 mm and a stiffness thickness of 2.0 mm.

**Table 1.** Chemical composition of STS304.

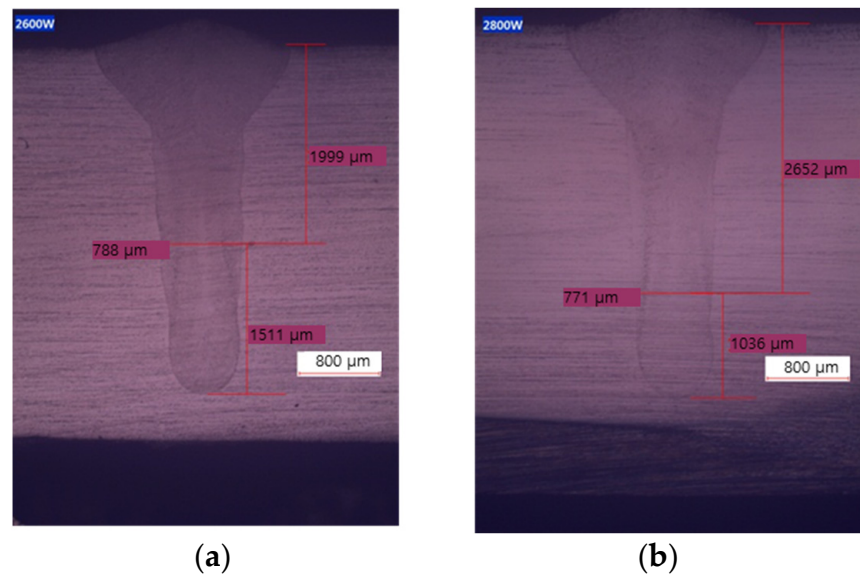
Chemical Composition	C	Si	Mn	P	S	Ni	Cr
Content (%)	0.08	≤1.0	≤2.0	≤0.045	≤0.03	8.0–10.5	18.0–20.0

**Table 2.** Laser welding condition.

Thickness (mm)		Laser Power (W)	Welding Speed (mm/min)
Skin	Stiffener		
2.0	-	2000	2000
2.67	-	2500	2000
2.0	2.0	2600	2000
2.67	2.0	2800	2000



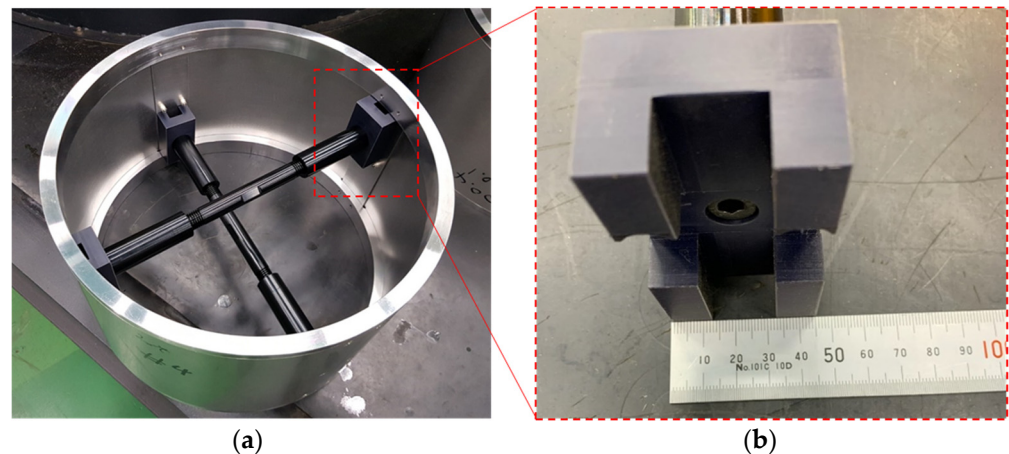
**Figure 7.** Photo of laser welding.



**Figure 8.** Cross-sectional macrograph of stiffener welding joints: (a) skin thickness: 2.0 mm + stiff. thickness: 2.0 mm; (b) skin thickness: 2.67 mm + stiff. thickness: 2.0 mm.

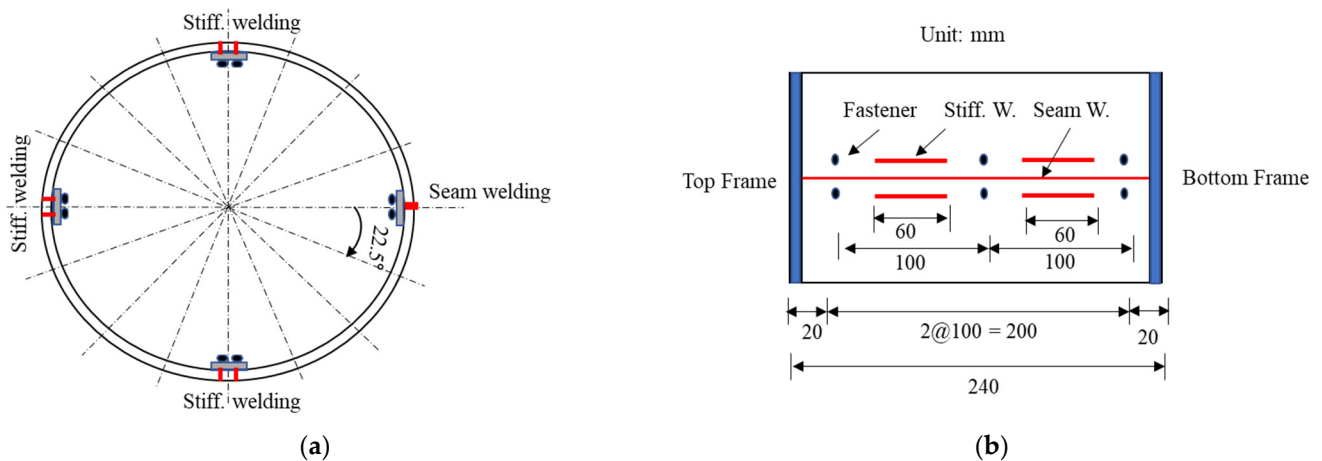
### 3.2. Deformation-Prevention Fixture and Welding Deformation Measurement

Figure 9 demonstrates a jig configured to induce tensile stress on the skin plate to prevent deformation. The jig is a straight structure, and grooves are installed on both ends to prevent interference with the stiffener on the back side of the welded part. Tensile stress is applied to the skin plate by rotating the screw installed in the centre of the jig to generate a forced displacement from the inside of the cylinder to the outside and elongate the jig. In the structure shown in Figure 9, two jigs are located across each other.



**Figure 9.** Picture of jig to give forced displacement: (a) full picture; (b) contact part of the jig.

Figure 10 demonstrates the location for the deformation measurement in the cylinder. The circumferential length was measured at intervals of  $22.5^\circ$  in a clockwise direction, using the seam-welded part as a reference point. The longitudinal distances were 20, 70, 120, 170, and 220 mm at five different positions. Figure 11 shows a touch-type deformation measuring device with a measurement error within  $5/1000$  mm.



**Figure 10.** Positions of welding deformation measurement: (a) circumferential direction; (b) welding length direction.

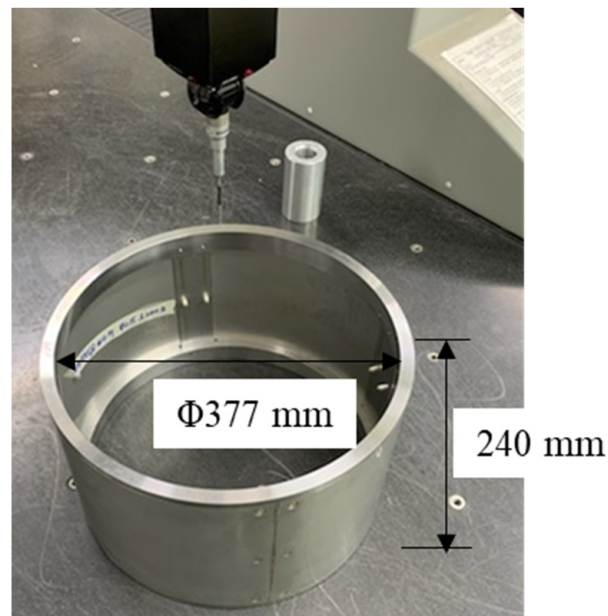


**Figure 11.** Welding-deformation measuring device.

## 4. Results and Discussion

### 4.1. Parametric Studies by Varying the Initial Stress

A thermo-elastoplastic analysis was performed to investigate the reduction in welding deformation as a function of the magnitude of the tensile stress applied on the skin plate. A forced displacement was imposed to expand the skin plate, and the tensile stress was set to 0, 50, 100, and 140 MPa [27].

Figure 12 demonstrates the temperature distribution in the cylindrical 1/4 model during welding. The thickness of the skin plate was 2.5 mm, and the laser welding heat was 2500 W. The heat source moved rapidly at the welding speed of 2000 mm/min, resulting in an increase in temperature around the welded part. The same temperature distribution was used for all specimens, regardless of the magnitude of the initial stress.

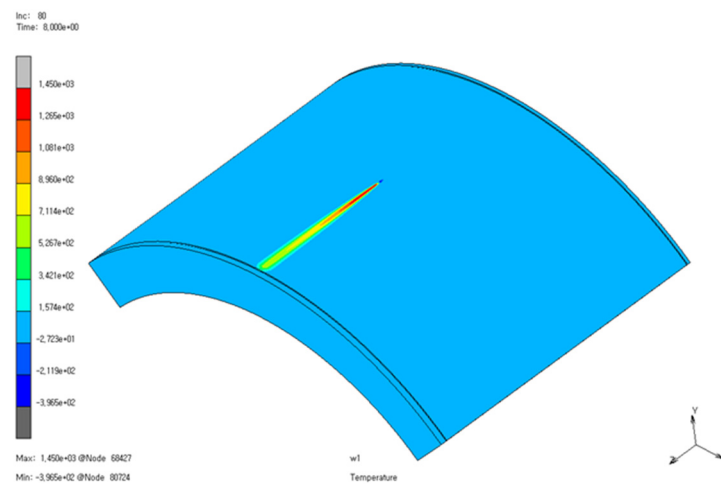


Figure 12. Welding temperature distribution at 8 s after welding started.

Figure 13 depicts the welding deformation in the absence of tensile stress. Initially, when tensile stress was not applied (Figure 13a), the temperature increased owing to the welding heat source; consequently, the skin plate expanded because of thermal expansion (Figure 13b). Subsequently, the material bent inside owing to the angular and longitudinal bending deformations during cooling. In general, angular deformation causes expansion of both sides around the welded part; however, when both sides are constrained, as in the case of the structure used in this analysis model, the sides cannot expand. Therefore, angular deformation occurs in the welded part, which is weak in terms of its rigidity, resulting in the inward bending of the sides of the material (Figure 13c).

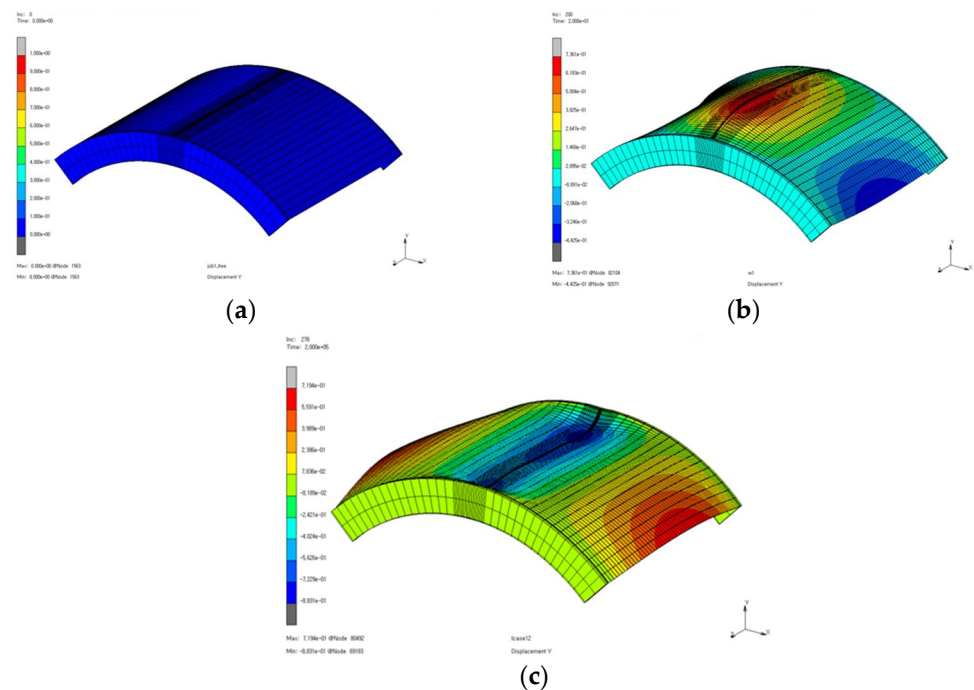
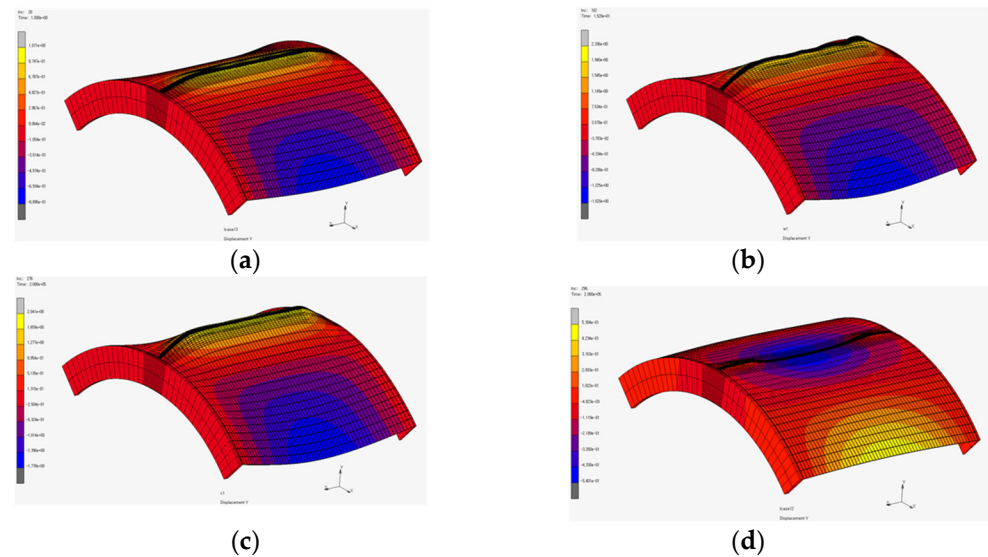


Figure 13. Welding deformation at tensile stress of 0 MPa: (a) initial conditions; (b) welding; (c) cooling after welding.

Figure 14 demonstrates welding deformation over time when a tensile stress of 100 MPa was induced on the skin plate by forced displacement, representing the four tensile stress analysis conditions (0, 50, 100, and 140 MPa) [27]. Initially, a tensile stress of approximately 100 MPa was induced on the skin plate (Figure 14a), which caused a slight swelling in the

skin plate. Subsequently, deformation occurred because of the expansion of the welded area caused by welding heat (Figure 14b). Figure 14c shows the deformation when the weld temperature reached room temperature after welding was completed. Figure 14d demonstrates the concave downward welding deformation in the environment when the forced displacement was removed once the weld was completely cooled.



**Figure 14.** Welding deformation at tensile stress of 100 MPa during: (a) forced displacement; (b) welding; (c) cooling after welding; (d) when forced displacement is removed [27].

Figure 15 shows the effect of the magnitude of the tensile stress on the final deformation. The final deformation was observed at the center of the welded part in the y-direction (radial direction). The deformation decreased linearly with increasing tensile stress. The final welding deformation barely occurred at 140 MPa, where the initial tensile stress was approximately 50% of the yield stress.

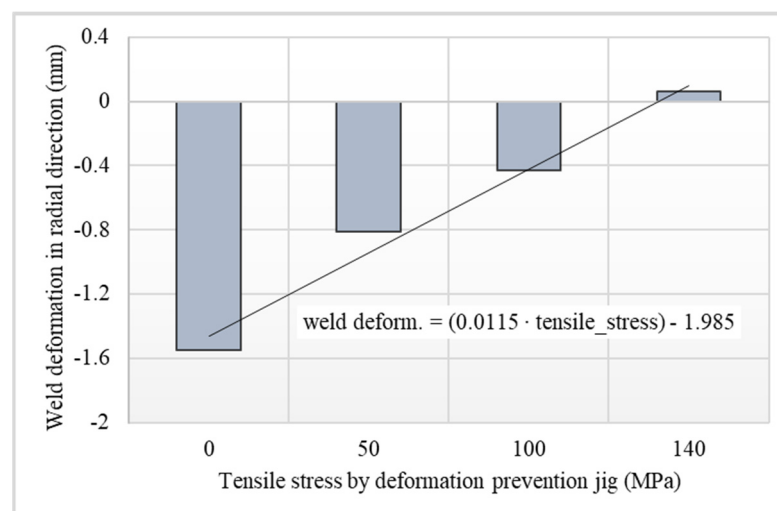


**Figure 15.** Final deformation of the center of welding line according to tensile stress.

#### 4.2. Application of the Tensile Stress Method to Cylindrical Structures

The thermo-elastoplastic analysis indicated the reduction in welding deformation when tensile stress was induced on the skin plate. This observation verified the reduction in welding deformation using the tensile stress method. The thicknesses of the skin plates were 2 and 2.67 mm. In addition, one seam and three bead-on welded parts were used. The

thermo-elastoplastic analysis suggested that the welding deformation could be completely controlled when the tensile stress was approximately 50% of the yield stress. However, seam welding caused significant deformation when a non-uniform and high tensile stress was induced by forced displacement during the experimental investigation, indicating that a high tensile stress cannot be applied. Therefore, a tensile stress of approximately 30 MPa was applied during the experiments.

Figure 16 demonstrates the effect of the jig on the welding deformation of a cylindrical structure with a skin plate thickness of 2 mm. The horizontal direction (x-axis) of the graph represents the angle, which is divided at intervals of  $22.5^\circ$  in the clockwise direction based on the seam-welded part. The vertical direction (y-axis) corresponds to the welding deformation. The  $0^\circ$  and  $360^\circ$  angles, shown on the horizontal axes, were seam-welds—whereas the stiffener and skin plate were bead-on welded at the other three positions ( $90^\circ$ ,  $180^\circ$ , and  $270^\circ$ ). The welding deformation was higher in the bead-on-plate weld than in the seam weld; this is because the bead weld was formed deep in the thickness direction of the seam weld and the shrinkage was higher than the angular deformation. In addition, the positions of  $z = 20$  and  $220$  mm were in close contact with the frames at both ends of the cylinder; therefore, welding deformation barely occurred at these positions.

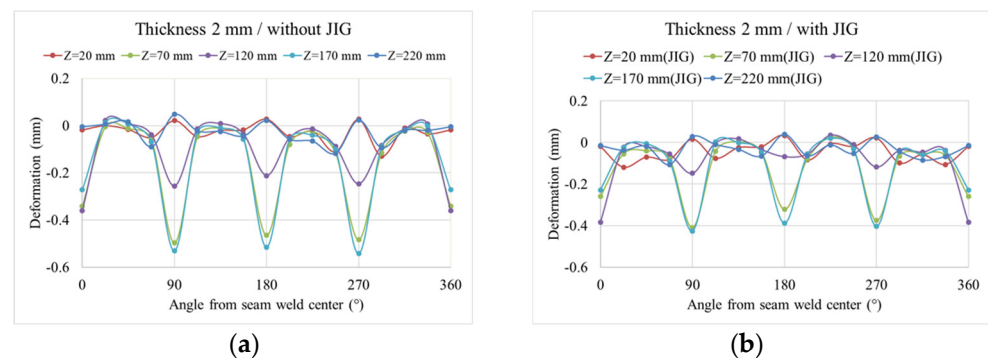


**Figure 16.** Weld deformation in the radial direction according to the circumferential direction at thickness 2 mm: (a) without jig; (b) with jig.

The deformation pattern in the longitudinal direction of the weld line is shown in Figure 16a. At  $0^\circ$  on the horizontal axis, a slight difference in deformation can be observed based on the position ( $z$  value); however, a significant difference in the magnitude of deformation was observed at  $90^\circ$ ,  $180^\circ$ , and  $270^\circ$ , based on different positions ( $z$  value). This was attributed to the absence of weld at the center ( $z = 120$  mm; Figure 10); however, the skin and back plates were welded at  $z = 70$  and  $170$  mm, respectively. A similar tendency was observed in all the specimens. When the thickness of the skin plate was 2 mm, welding deformation of up to 0.5 mm occurred inside the cylinder in the absence of an anti-deformation jig. In contrast, approximately 0.4 mm of deformation occurred when the anti-deformation jig is used. Thus, welding deformation was reduced by 20% by using the pre-stress method.

Figure 17 shows the effect of an anti-deformation jig on the welding deformation when the thickness of the skin plate was 2.67 mm. A maximum of 0.45 mm of welding deformation was observed in the absence of an anti-deformation jig. In contrast, a welding deformation of approximately 0.4 mm was observed when an anti-deformation jig was installed. Thus, the welding deformation was reduced by 11% at a tensile stress of 30 MPa. In the case of a tensile stress of 30 MPa, the 11% reduction effect in the experiment obtained a very similar result to the 17% reduction effect in the thermo-elastoplastic analysis—as shown in Figure 15. Therefore, the experimental studies confirmed that welding deformation can be reduced by introducing pre-stress using an anti-deformation jig.

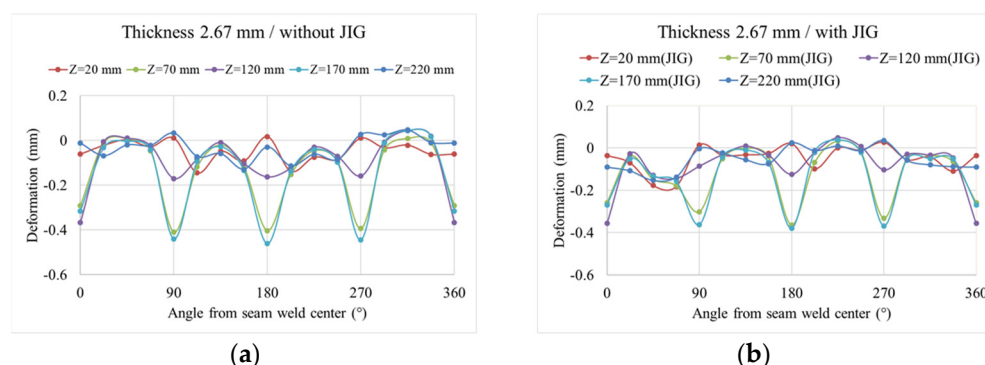


**Figure 17.** Weld deformation in the radial direction according to the circumferential direction at thickness 2.67 mm: (a) without jig; (b) with jig.

## 5. Conclusions

An anti-deformation device was developed to reduce welding deformation during the manufacturing of a cylindrical structure made of STS304 by laser welding. The effect of tensile stress was investigated on the welding deformation. The major conclusions are as follows:

1. Seam-welding deformation of the cylinder was caused by angular and longitudinal deformations. The shape of the deformation was characterized by the downward bending at the part with a relatively low stiffness.
2. The skin plate was expanded using an anti-deformation jig, and tensile stress was induced at the welded area to reduce welding deformation. The tensile stress induced by the anti-deformation jig assisted in increasing the thermal stress caused by the welding heat, thereby reducing the amount of compression plastic deformation and, consequently, reducing the welding deformation.
3. Thermo-elastoplastic analysis confirmed the effects of tensile stress on welding deformation. Welding deformation did not occur when the tensile stress was approximately 50% of the yield stress of the base metal.
4. When a tensile stress of 30 MPa was applied to an actual cylinder, welding deformation was reduced by 11–20% compared to that without applying tensile stress.

**Author Contributions:** Conceptualization and investigation, H.-C.J.; writing—original draft preparation and writing—review and editing, S.-H.L. and J.-U.P. All authors have read and agreed to the published version of the manuscript.

**Funding:** This study was supported by a research fund from the Chosun University (2021) and the Agency for Defense Development by the Korean Government (UC189015CD).

**Data Availability Statement:** Not applicable.

**Conflicts of Interest:** The authors declare no conflict of interest.

## References

1. Masubuchi, K. *Analysis of Welded Structures: Residual Stresses, Distortion, and Their Consequences*; Elsevier: Amsterdam, The Netherlands, 2013; Volume 33.
2. Ma, N.; Huang, H.; Yin, X.; Guo, N. Welding distortion and inherent deformation under temporary tacking and its released states. *Sci. Technol. Weld. Join.* **2016**, *21*, 389–396. [[CrossRef](#)]
3. Farzaneh, A.; Khorasani, M.; Farabi, E.; Gibson, I.; Leary, M.; Ghasemi, A.; Rolfe, B. Sandwich structure printing of Ti-Ni-Ti by directed energy deposition. *Virtual Phys. Prototyp.* **2022**, *17*, 1006–1030. [[CrossRef](#)]
4. Liang, X.; Dong, W.; Hinnebusch, S.; Chen, Q.; Tran, H.T.; Lemon, J.; Cheng, L.; Zhou, Z.; Hayduke, D.; To, A.C. Inherent strain homogenization for fast residual deformation simulation of thin-walled lattice support structures built by laser powder bed fusion additive manufacturing. *Addit. Manuf.* **2020**, *32*, 101091. [[CrossRef](#)]
5. Li, W.; Li, S.; Liu, J.; Zhang, A.; Zhou, Y.; Wei, Q.; Yan, C.; Shi, Y. Effect of heat treatment on AlSi10Mg alloy fabricated by selective laser melting: Microstructure evolution, mechanical properties and fracture mechanism. *Mater. Sci. Eng. A* **2016**, *663*, 116–125. [[CrossRef](#)]

6. Xie, Z.; Wu, M.; Shi, X.; Lu, P.; Miao, X. Study on the forming precision optimization of built-in flow channel structure manufactured by selective laser melting. *Proc. Inst. Mech. Eng. Part B J. Eng. Manuf.* **2022**, 0954405422111897. [[CrossRef](#)]
7. Dar, N.U.; Qureshi, E.M.; Hammouda, M. Analysis of weld-induced residual stresses and distortions in thin-walled cylinders. *J. Mech. Sci. Technol.* **2009**, *23*, 1118–1131. [[CrossRef](#)]
8. Ahn, J.T.; Shin, D.K. Ultimate Flexural Strength of Cylindrical Steel Shell for Wind Tower. *J. Korean Soc. Steel Constr.* **2015**, *27*, 109–118. [[CrossRef](#)]
9. Tsai, C.; Park, S.; Cheng, W. Welding distortion of a thin-plate panel structure. *Weld. J. NY* **1999**, *78*, 156s–165s.
10. Javadi, Y.; Hasani, M.; Sadeghi, S. Investigation of Clamping Effect on the Welding Sub-surface Residual Stress and Deformation by Using the Ultrasonic Stress Measurement and Finite Element Method. *J. Nondestruct. Eval.* **2015**, *34*, 3. [[CrossRef](#)]
11. Deo, M.V.; Michaleris, P. Mitigation of welding induced buckling distortion using transient thermal tensioning. *Sci. Technol. Weld. Join.* **2003**, *8*, 49–54. [[CrossRef](#)]
12. Park, J. Prevention and orrection of welding deformation. *J. Weld. Join.* **2005**, *23*, 323–326.
13. Park, J. Effect of Forced Cooling condition along with Welding on Welding Angular Distortion. *J. Korea Acad.-Ind. Coop. Soc.* **2013**, *14*, 2021–2026. [[CrossRef](#)]
14. Jeong-ung Park, G.A.; Seung-hyun, Y. Prediction and Welding Sequence of Minimum Welding Deformation in Large Steel Block Welding. *J. Weld. Join.* **2017**, *35*, 8–14. [[CrossRef](#)]
15. Kim, H.-G.; Lee, M.; Shin, S.B. A Study on the Distortion Control Characteristics of the STS 304 Multi-pass Butt Weldment by Tensioning Method. *J. Korean Weld. Join. Soc.* **2010**, *28*, 73–78. [[CrossRef](#)]
16. Zhang, L.J.; Zhang, J.X.; Liang, W.; Serizawa, H.; Murakawa, H. Numerical Study on the Effectiveness of Fixture and Pre-Strain for Reduction of Welding Distortion. In *Materials Science Forum*; Trans Tech Publications Ltd.: Zurich, Switzerland, 2008; pp. 401–404.
17. Rupani, S.; Barai, A. Influence of Welding Sequence on Distortion of Circumferential Pipe Joint—A Review. *J. Prod. Res. Manag.* **2016**, *6*, 1–5.
18. Seong, W.-J.; Chun, K.-S. Welding Deformation and Its Correction of Cylindrical Moon Pool Structure. *J. Soc. Nav. Archit. Korea* **2019**, *56*, 389–395. [[CrossRef](#)]
19. Park, J.-U.; Lee, H.-W.; Bang, H.-S. Effects of mechanical constraints on angular distortion of welding joints. *Sci. Technol. Weld. Join.* **2002**, *7*, 232–239. [[CrossRef](#)]
20. Ma, N.; Huang, H. Efficient Simulation of Welding Distortion in Large Structures and Its Reduction by Jig Constraints. *J. Mater. Eng. Perform.* **2017**, *26*, 5206–5216. [[CrossRef](#)]
21. Nishimura, R.; Ma, N.; Liu, Y.; Li, W.; Yasuki, T. Measurement and analysis of welding deformation and residual stress in CMT welded lap joints of 1180 MPa steel sheets. *J. Manuf. Process.* **2021**, *72*, 515–528. [[CrossRef](#)]
22. Liu, Y.; Ma, N.; Lu, F.; Fang, H. Measurement and analysis of welding deformation in arc welded lap joints of thin steel sheets with different material properties. *J. Manuf. Process.* **2021**, *61*, 507–517. [[CrossRef](#)]
23. Seyedian, C.M.; Haghpanahi, M.; Sedighi, M. Investigation of the effect of clamping on residual stresses and distortions in butt-welded plates. *Sci. Iran.* **2010**, *17*, 387–394.
24. Schenk, T.; Richardson, I.; Kraska, M.; Ohnimus, S. A study on the influence of clamping on welding distortion. *Comput. Mater. Sci.* **2009**, *45*, 999–1005. [[CrossRef](#)]
25. Hammad, A.; Churiaque, C.; Sánchez-Amaya, J.M.; Abdel-Nasser, Y. Experimental and numerical investigation of hybrid laser arc welding process and the influence of welding sequence on the manufacture of stiffened flat panels. *J. Manuf. Process.* **2021**, *61*, 527–538. [[CrossRef](#)]
26. Liu, Y.; Wang, P.; Fang, H.; Ma, N. Mitigation of residual stress and deformation induced by TIG welding in thin-walled pipes through external constraint. *J. Mater. Res. Technol.* **2021**, *15*, 4636–4651. [[CrossRef](#)]
27. Lee, S.-H.; Lee, D.-O.; Park, K.-S.; Jeon, H.-C.; Kim, S.-T.; Park, J.-U. Laser Welding Deformation Control of STS304 Cylindrical Steel Sheet Structure. *J. Weld. Join.* **2020**, *38*, 521–527. [[CrossRef](#)]
28. MSC Team. *Marc Mentat 2015 User Guide Documentation*; MSC Software Corp.: Los Angeles, CA, USA, 2015.
29. Goldak, J.; Chakravarti, A.; Bibby, M. A new finite element model for welding heat sources. *Metall. Trans. B* **1984**, *15*, 299–305. [[CrossRef](#)]

**Disclaimer/Publisher’s Note:** The statements, opinions and data contained in all publications are solely those of the individual author(s) and contributor(s) and not of MDPI and/or the editor(s). MDPI and/or the editor(s) disclaim responsibility for any injury to people or property resulting from any ideas, methods, instructions or products referred to in the content.